Simancas, R.; Nishitoba, T.; Park, S.; Kondo, JN.; Rey Garcia, F.; Gies, H.; Yokoi, T. (2021). Versatile phosphorus-structure-directing agent for direct preparation of novel metallosilicate zeolites with IFW-topology. Microporous and Mesoporous Materials. 317:1-10. https://doi.org/10.1016/j.micromeso.2021.111005

Versatile Phosphorus-Structure-Directing Agent for Direct Preparation of Novel Metallosilicate Zeolites with IFW-topology

Raquel Simancas*[a1], Toshiki Nishitoba[a], Sungsik Park[a], Junko N. Kondo[a], Fernando Rey[b], Hermann Gies[c,d], Toshiyuki Yokoi*[a, d]

a Institute of Innovative Research, Tokyo Institute of Technology, 2268503, Japan.

b Instituto de Tecnología Química (UPV-CSIC) Universitat Politècnica de València - Consejo Superior de Investigaciones Científicas, 46022, Spain.

c Institute of Geology, Mineralogy und Geophysics, Ruhr-University Bochum, 44780, Germany.

d Tokyo Tech World Research Hub Initiative (WRHI), Institute of Innovative Research, Tokyo Institute of Technology, 2268503, Japan.

Email: rsimancas@chemsys.t.u-tokyo.ac.jp, yokoi@cat.res.titech.ac.jp

Abstract

To fabricate a novel metallosilicate zeolite with a tridirectional pore system of 8- and 10-ring channels, direct incorporation of B, Al and Ga into small and medium pore ITQ-52 zeolite with the IFW-type topology was carried out using a phosphorus-containing organic structure-directing agent (P-OSDA, 1,4-butanediylbis[tris(dimethylamino)]phosphonium hydroxide). The solids were characterized by XRD, FT-IR, ^{11}B, ^{27}Al, ^{31}P and ^{71}Ga MAS NMR spectroscopy before and after post-synthesis treatments and steaming. It was found that the P-species derived from OSDA were decomposed by heat treatments, forming extra-framework phosphates that remain in the cavities of the zeolite. The presence of P-species not only stabilized the Al or Ga located in framework positions which adopted a reversible octahedral configuration but also decreased the acid strength of the zeolites. The catalytic performance of the Al- and Ga-

containing ITQ-52 zeolites in the MTO reaction was investigated. We have found that the presence of P in ITQ-52 enhanced the catalytic life time, and that the optimum P content for the samples with Si/Al = 120 and Si/Ga = 135 were found to be P/Al = 0.17 and P/Ga = 0.14, respectively, showing a propene selectivity higher than 35%.

Keywords

B-, Al- and Ga-containing zeolite; acid strength; Phosphorus modification; methanol to olefins; hydrothermal stability

1. Introduction

Zeolites are one of the most studied functional materials, with wide applications in adsorption, ion exchange and catalysis fields.[1][2] The number of new structures is increasing every year, having recognized 253 different frameworks by the International Zeolite Association (IZA) up to date.[3] The synthesis of the zeolitic materials is usually assisted by organic structure-directing agents (OSDAs). Tetraalkylammonium cations are the most common OSDAs but other organic molecules, such as aza- and oxo-crown macrocycles, proton sponges, metal complexes, alkylphosphonium, sulfonium and arsonium cations, have also been described for zeolite synthesis.[4][5] Phosphorus-containing compounds were started to use as OSDA in the ’70s, allowing the synthesis of already known zeolites such as ZSM-5 or ZSM-11. [6][7]. The use of a mixture of tetraethylphosphonium cations and the corresponding alkylammonium OSDA has allowed preparing some small pore zeolites.[8][9][10] Besides, several new zeolites of different pore size and dimensionality have also been obtained by using tetraalkylphosphonium cations as OSDA. [11][12][13][14][15]. Furthermore, the synthetic natural analogue of the large and medium pore boggsite zeolite (ITQ-47) was prepared by using a phosphorus-proton sponge.[16]

Tetraalkylphosphonium cations do not suffer Hofmann elimination showing better thermal stability than tetraalkylammonium cations and allowing the crystallization of zeolites under more severe conditions. The phosphorus-containing cations not only work as a versatile OSDA but also allow to introduce extra-framework P-species during the synthesis that remain as phosphates in the pores and channels of the zeolites upon the heating treatments of the solids. This is especially important for the small pore zeolites, which presents a pore aperture too small for introducing P by standard post-synthesis methods. The presence of those extra-framework P-species has a twofold effect on the aluminosilicates, modifying the acid properties of the catalyst while increasing the stability of the Al atoms in tetrahedral coordination in framework position during reaction or regeneration conditions, where high temperatures in the presence of steam are frequently used.[17][18][19]

The zeolite ITQ-52 (IZA code IFW) is an example of a new structure-type prepared by using a phosphorus-containing cation as OSDA (1,4-butanediylbis[tris(dimethylamino)] phosphonium hydroxide, P-OSDA).[20] The IFW phase presents a tridirectional pore system of 8- and 10-ring channels that intersect one to each other creating large cavities, accessible through two 10R and four 8R apertures. Later, the same structure was reported by using the *N,N´*-diisopropyl-*N,N´*-diethylbicyclo[2.2.2]oct-7-ene-2,3:5,6-dipyrrolidinium dication as OSDA obtaining the zeolite SSZ-87.[21] In both cases, the synthesized materials were borosilicates. The preparation of the Al-containing material will open the study of the catalytic activity of this zeolite.

Herein, we report the direct synthesis of the IFW-type metallosilicate zeolites, B, Al and Ga-containing zeolite ITQ-52, by using 1,4-butanediylbis[tris(dimethylamino)]phosphonium hydroxide as P-OSDA. The interaction of the extra-framework phosphates formed during the heat treatments with the Al and Ga atoms located in framework positions will be studied by solid-state NMR spectroscopy. While the influence of the presence of P-species inside the

cavities of the zeolite on the adsorption and acid properties as well as its performance in the methanol to olefins (MTO) reaction will be discussed

2. Experimental

2.1. Synthesis of Al and Ga-containing ITQ-52 zeolite

The ITQ-52 zeolites were prepared by using the compound 1,4-butanediylbis[tris(dimethylamino)] phosphonium hydroxide as P-OSDA. The organic molecule was prepared as previously described in the literature.[20] In a typical zeolite synthesis, 0.309 g of H_3BO_3 (Aldrich) and 15.583 g of tetraethylorthosilicate (TEOS, Aldrich) were added to a 61.539 g of a 0.26M aqueous solution of the OSDA. The mixture was stirred at room temperature for 24 h. The water content was adjusted until obtaining the appropriate composition. Then, 1.333 g of HF (48 wt% in H_2O, Aldrich) were added. The solidified mixture was manually stirred for 5 min. The final synthesis gel with the following molar composition 0.935 SiO_2 : 0.0325 B_2O_3 : 0.2 $OSDA(OH)_2$: 0.4 HF : 7.5 H_2O was transferred to Teflon lined stainless-steel autoclaves and heated at 423 K at its autogenous pressure under tumbling (40 rpm) for 5 days. The solid was recovered by filtration and washed exhaustively with distilled water. The resulting solid was dried at 373 K overnight to obtain the as-made [B]-ITQ-52.
The Al- and Ga-containing zeolites were prepared following the previous synthesis procedure, but $Al(OH)_3$ (Aldrich) and $Ga(NO_3)_3$ (Aldrich), used as Al and Ga sources, respectively, were dissolved in the aqueous mixture after the addition of TEOS. Also, before the incorporation of HF, some crystals of the as-made [B]-ITQ-52 were added as seeds (4 wt% relative to SiO_2). The zeolites were prepared from a synthesis gel with the following composition 0.935 SiO_2 : (0.0325-x) B_2O_3 : x T_2O_3 : 0.2 $OSDA(OH)_2$: 0.4 HF : 7.5 H_2O : 0.04 Seeds, where, T_2O_3 is Al_2O_3 or Ga_2O_3, and x varies from 0.0025 to 0.0325.

2.2. Post-synthesis treatments

The as-made materials were heated at 923 K under air or 873 K under a stream of 20% (v/v) of H_2 in N_2 and then at 923K under air. Some materials were subsequently submitted to a washing treatment consisting in the heating of the zeolite ITQ-52 in a 3M aqueous ammonium acetate solution at 303 – 363 K for 2 hours and calcined at 823 K under air. Phosphorus wet impregnation was carried out on the washed samples by using the proper amount of an aqueous H_3PO_4 solution at room temperature and calcination at 823 K under air. The steaming treatment was performed in the sieved sample at 973 K for 5 hours using a water flow rate of 1 $\mu l \cdot min^{-1} \cdot (g\text{-zeolite})^{-1}$ diluted in 100 $mL \cdot min^{-1}$ of N_2.

Precaution: During the heating under a stream of H_2/N_2, phosphines are formed, it is necessary to use a trap with an aqueous $Cu(NO_3)_2$ solution for trapping the reduction products.

2.3. Characterization

The XRD patterns were collected on a Rint-Ultima III (Rigaku) X-ray diffractometer using Cu K_α radiation at 40 kV and 40 mA. The chemical composition was determined by using an inductively coupled plasma-atomic emission spectrometer ICP-AES, Shimadzu ICPE-9000. Field-emission scanning electron microscopy (FESEM) images were obtained on a Hitachi SU9000 microscope at an accelerating voltage of I.0 kV. The thermogravimetric profiles were recorded on a thermogravimetric-differential thermal analyser TG-DTA, RigakuThermo plus EVO II. The IR spectra of the zeolite using CO and pyridine as probe molecule were recorded in a JASCO FT/IR-6100 spectrometer at 153 K and 423 K, respectively. The self-supporting wafers of 20 mm of diameter and around 50 mg of weight were pre-treated at 673K under vacuum for 1 h. The CO was adsorbed and desorbed at 153 K. While the pyridine was adsorbed in the zeolite at 423 K and desorbed under vacuum at 423, 523 and 623 K. Solid NMR spectra were acquired in a JEOL ECA-600 spectrometer. Ammonia desorption profiles were recorded on a MicrotacBEL

Multitrack TPD equipment. N_2 adsorption isotherms were obtained at 77 K in a BELSORP max Bel Japan. The samples were evacuated at 673 K for 12 h before the measurement.

2.4. Catalytic tests

The MTO reaction was carried out on a fix reactor. Around 100 mg of 50-100 mesh zeolite pellets were loaded in a 6 mm quartz tubular flow microreactor. The catalysts were activated at 773 K in Ar flow prior to the reaction. The MeOH was fed by a Harvard Apparatus syringe pump, mixed with Ar stream in a preheater and introduced in the catalyst bed. The reaction was performed at 673 K with a flow rate of WHSV = 0.5 h^{-1} and a methanol pressure of 5 kPa. The product stream was analysed by FID on a GC-2014 equipped with an HP-PLOT/Q capillary column. Product selectivities were calculated on the carbon number basis.

3. Results and discussion

3.1. Incorporation of Al and Ga in the zeolite ITQ-52

The zeolite ITQ-52 (IFW) has been prepared as borosilicate in basic and fluoride media using the phosphorus-containing cation 1,4-butanediylbis[tris(dimethylamino)]phosphonium hydroxide.[20] Zeolite ITQ-52 frequently crystallizes with ITQ-58 [22] and STF-type[23] zeolites, being far from being trivial to obtain it as pure phase. The synthesis in the presence of fluoride media avoids the formation of ITQ-58, therefore, all syntheses described in this paper were carried out in fluoride media.

The direct incorporation of Al in the zeolite ITQ-52 was attempted several times yielding to mixtures of ITQ-52 and STF-type phases (Figure S1). Thus, seeding using as-made [B]-ITQ-52 was attempted to increase the crystallization rate of ITQ-52 versus the competing phase as has been reported for other zeolites.[24][25]. The syntheses were carried out by keeping the

Si/trivalent ratio at 15 (Si/(B+Al) = 15). All the obtained solids show the characteristic diffraction pattern of the IFW phase (Figure S2).

The zeolite ITQ-52 was obtained from a Si/Al ratio of 17.8 to pure borosilicate, whilst keeping a Si/T(III) very close to 18. The chemical analysis and unit cell volume of the solids are shown in Table 1. The [Al_19]-ITQ-52 was prepared by using the sample [B,Al_21]-ITQ-52 as seed instead of [B]-ITQ-52, by doing this, the amount of B found in the final solid was negligible. The incorporation of trivalent elements (B, Al or Ga) in the framework generates a negative charge that is compensated by the cationic OSDA. The chemical analyses show 4 phosphorus atoms per unit cell that corresponds to 2 OSDA molecules per unit cell or 1 OSDA per cavity. The Si/trivalent ratio of the final solids was close to 18, that is the needed value to compensate the positive charges introduced in the framework by the presence of the OSDA. When the Si/trivalent ratio was changed in the synthesis gel, the pure IFW-type phase was not obtained (Figure S1). Indicating that despite of structure-directing effect of the organic cation, the charge density mismatching[26] inhibits ITQ-52 crystallization.

It was noticed that some diffraction peaks in the XRD patterns of the as-synthesized [B,Al]-ITQ-52 zeolites shift towards higher d-spacings as Al was increased in the synthesis media. For studying this phenomenon, the XRD patterns were indexed with a monoclinic unit cell using the program DICVOL[27] integrated into the suite of programs FULLPROF[28]. The unit cell parameters of the zeolites are listed in Table S1. The unit cell parameters change with the composition of the zeolite, showing a larger elongation for the *a* and *b* parameters than for the *c* with the Al content (Figure 1). Whereas the unit cell volume shows a linear correlation with the Al atoms per unit cell, suggesting the incorporation of Al in framework positions.

The chemical environment of the B, Al and P atoms in the obtained solids was studied by solid-state NMR spectroscopy. Figure 2a shows the ^{11}B, ^{27}Al and ^{31}P MAS NMR spectra of the as-made [B,Al_91]-ITQ-52, the NMR spectra of samples with different Al content are shown in

Figure S3. All the samples show a narrow resonance at -3.8 ppm in the ^{11}B MAS NMR spectra assigned to tetrahedral boron in framework positions.[29]. The ^{27}Al MAS NMR spectrum confirms the incorporation of the tetrahedral Al in framework positions, being absent any resonance centred at 0 ppm characteristic of the octahedrally coordinated species. The observation of two resonances at 54 and 56 ppm indicates the presence of Al in two different environments in tetrahedral coordination. The existence of several resonances in that region has been also attributed to aluminium located at different non-equivalent framework positions.[30][31] In a previous work, the preferential location of the boron atoms in 2 of the 10 different T sites of the borosilicate IFW-type was described.[21] The presence of at least two different resonances in the ^{27}Al MAS NMR spectra suggests the non-random siting of the Al in the ITQ-52 zeolite, however, the incorporation in preferred location cannot be controlled by synthesis. Finally, the single resonance observed in the ^{31}P MAS NMR spectrum at 61 ppm indicates that the intact OSDA is located inside the zeolite cavities.

The synthesis of the Ga-containing ITQ-52 was attempted following a similar strategy. The incorporation of Ga was more difficult, this could be explained with the larger size of Ga (r=0.47Å) compared with B (r=0.11Å) and Al (r=0.39Å)[32]. The pure ITQ-52 zeolite was prepared with a Si/Ga ratio up to 71, while mixtures of ITQ-52, STF-type and amorphous solid were obtained when the Ga content was increased in the synthesis media (Figure S1 and S4). The chemical analyses and unit cell volume of Ga-containing ITQ-52 zeolites are shown in Table 1. As in the [Al]-ITQ-52 case, the Si/trivalent ratio was close to 18 and 2 OSDA molecules per unit cell were found. Besides, the unit cell volume increases with the Ga content, suggesting the incorporation of Ga in framework positions.

The ^{11}B, ^{71}Ga and ^{31}P MAS NMR spectra of the as-synthesized [B,Ga_82]-ITQ-52 are shown in Figure 3a, NMR spectra of as-made samples with different Ga content can be found in Figure S5. The ^{11}B and ^{31}P MAS NMR spectra of the [B,Ga_82]-ITQ-52 are very similar to those

obtained for the [B,Al_91]-ITQ-52. While, the ^{71}Ga MAS NMR spectra show a broad resonance centred at 169 ppm, assigned to tetrahedral Ga incorporated in framework positions.[33] The zeolite [B]-ITQ-52 crystallizes forming rectangles prims of 2 x 0.8 x 0.6 μm (Figure S6), that are slightly larger than the previously reported crystal sizes.[20] This difference is attributed to the influence of the crystallization media on the crystal growth, the [B]-ITQ-52 described in this manuscript was synthesized using fluoride anions as mineralizing agent that frequently leads to the formation of large crystals.[34] The incorporation of Al in the synthesis gel resulted in plate-like crystals agglomerated in prims of a similar size to [B]-ITQ-52 particles. While, the [B,Ga_97]-ITQ-52 crystals are very similar to those obtained for the [B]-ITQ-52.

3.2. Evolution of the B, Al, Ga and P species during the thermal treatments

The Al and Ga-containing ITQ-52 samples were treated at high temperature to decompose the OSDA. The heating under air decomposes the OSDA cations in NO_x, CO_2 and H_2O molecules that diffuse out of the solid and also, P_xO_y species are formed that remain in the cavities of the zeolite ITQ-52, showing a P/u.c. very similar to that obtained for the as-made sample (Table S2). On the other hand, upon the reduction treatment by heating under a stream of H_2/N_2, the OSDA decomposition cannot lead to oxidized species, and phosphorus is partially removed as volatile phosphines. Thus, close to 50 wt% of the incorporated P by the OSDA remained as P_xO_y after the second heat treatment under air, in this case, for burning some carbon deposits generated during the reduction treatment.

Finally, more than 90 wt% of the original phosphorus can be removed by washing the zeolite in an aqueous ammonium acetate solution. However, the phosphorus washing was more effective after the heat treatment under H_2/N_2 flow than in air. It is remarkable that the trivalent cation content in the zeolites barely changed during the different treatments. Furthermore, the zeolite framework presents good stability, showing the characteristic

diffraction pattern of the IFW phase and comparable peak intensities before and after the post-synthesis treatments (Figure S7).

Solid-state NMR spectroscopy was employed to study the nature of the B, Al, Ga and P species after the different treatments. The ^{11}B, ^{27}Al and ^{31}P MAS NMR spectra of the [B,Al_91]-ITQ-52 as-made and after post-synthesis treatments, are shown in Figure 2. The ^{11}B MAS NMR spectra of all solids show a main resonance centred at -3.8 ppm, assigned to tetrahedral B located in framework positions. The low intense resonance centred at 20 ppm observed in the sample after the washing with the aqueous ammonium acetate solution and calcination is associated with the presence of a very minor fraction of B as extra-framework species.[29]

In the ^{31}P MAS NMR spectra of the heated samples in air or under a H_2/N_2 stream, [B,Al_91]-ITQ-52_AT and [B,Al_91]-ITQ-52_HT, respectively, can be distinguished four different resonances which intensity varies with the composition of the zeolite. The resonance centred at 0 ppm is assigned to extra-framework monomeric phosphate groups. While the resonances at -6 and -10 ppm are associated with the presence of pyrophosphoric acid and short-chain polyphosphates or pyrophosphates, respectively.[17][35] Finally, the broad resonance centred at -15 ppm is attributed to polymeric phosphate species interacting with the Al species that appear at -12 ppm in the ^{27}Al MAS NMR.[35] Although this region is characteristic for the Al in octahedral coordination, the Al atom remained in the framework. Upon the total removal of the extra-framework P-species by the treatment of the sample at 363 K with the aqueous ammonium acetate solution and subsequently calcination at 823 K, the resonance centred at –12 ppm disappeared, increasing the intensity of that assigned to the tetrahedral Al, also a minor resonance centred at 0 ppm corresponding to extra-framework Al species formed during the calcination of the zeolite is observed. This NMR results clearly indicate the Al can adopt a reversible octahedral coordination in the presence of extra-framework P species.

For checking the reversibility of this phenomenon, a zeolite ITQ-52 ([Al_20]-ITQ-52) was heated under H_2/N_2, washed with an ammonium acetate solution for removing the P species, and calcined, afterwards, the zeolite was wet impregnated with two different P content (1.25 and 2.50 wt%, corresponding to 1.7 and 3.1 P/u.c.) by using H_3PO_4 solutions. The ^{27}Al and ^{31}P MAS NMR spectra of all the zeolites are shown in Figure S8. The ^{31}P MAS NMR spectra of the impregnated samples show a broad resonance from 0 to -50 ppm, similar to that obtained upon the heat treatments of the [Al_20]-ITQ-52. The ^{27}Al MAS NMR spectra reflect the intensity increase of the resonance centred at -15 ppm with the phosphorus content, confirming the reversible octahedral coordination of the Al. However, a small amount of octahedral Al at 0 ppm is visible even the P/Al ratio is higher than 1. This extra-framework Al species were formed during the calcination of the washed samples and cannot revert to framework positions.

The Ga-containing ITQ-52 zeolite was also studied by MAS NMR spectroscopy, the ^{11}B, ^{71}Ga and ^{31}P MAS NMR spectra of the [B,Ga_82]-ITQ-52 as-made and after post-synthesis treatments, are shown in Figure 3. The results obtained in the ^{31}P and ^{11}B MAS NMR spectra were analogous to those observed for the [B,Al_91]-ITQ-52. Whereas the ^{71}Ga MAS NMR spectra show two resonances, the first one centred at 169 ppm corresponds to framework Ga in tetrahedral coordination, while the second one appears at -34 ppm, that is the characteristic region of Ga in octahedral coordination.[33] As for the previous case, the relative intensity of this resonances changes with the P content, recovering the intensity of the resonance at 169 ppm after removing the extra-framework phosphorus. This study suggests the reversible octahedral coordination in the presence of extra-framework P species is not only characteristic of the Al, but can also be observed in other trivalent atoms such as Ga.

3.3. Influence of the presence of extra-framework P-species in the textural and acid properties of the zeolite

The influence of the presence of extra-framework P species in the acid and textural properties of the zeolite ITQ-52 was studied in a series of samples having a Si/Al ratio of 20 and different P/Al ratios prepared by heat treatment under a stream of H_2/N_2 or in air and subsequent washing with an aqueous ammonium acetate solution at 303 or 363 K (table 2).

The acidity of the ITQ-52 zeolites was measured using FT-IR spectroscopy using pyridine and CO as probe molecules. Zeolite acidity was calculated from the integrated absorbance of the band corresponding to pyridine adsorbed in Brönsted (1550 cm^{-1}) and Lewis (1450 cm^{-1}) acid sites using the molar extinction coefficients previously reported by C. A Emeis.[36] The amount of adsorbed pyridine decreases with the P content, however, the samples having P/Al ratio 0.47 and 0.08 show a similar number of Brönsted acid sites at 423 K. This result can be explained by the presence of extra-framework Al species in the sample with the lowest P content as previously detected by ^{27}Al MAS NMR, and therefore these species could be responsible for the high concentration of Lewis acid sites in this sample.

Figure 4 shows the FT-IR spectra of the ITQ-52 zeolites having different P content using CO as probe molecule. The hydroxyls groups are sensitive to the CO interaction showing a band shift related to the acid strength of the OH groups.[37] All the samples show a shift of the acidic OH group from 3615 to 3296 cm^{-1} ($\Delta\nu$(OH) = 319 cm^{-1}) considered strong Brönsted acidity. The samples containing extra-framework P species also show a second shift of the OH groups corresponding to P-OH from 3655 to 3435 cm^{-1} ($\Delta\nu$(OH) = 220 cm^{-1}), attributed to medium-weak acidity. The presence of P not only introduces medium-weak acid sites but also decreases the number of strong Brönsted acid sites in the catalyst. In the CO vibration region, a main band centred at 2174 cm^{-1} assigned to the stretching vibration of $\nu(C\equiv O)$ on Brönsted acid sites is observed for all the samples. While the intensity of the band centred at 2224 cm^{-1}, that is

associated with the stretching vibration of ν(C≡O) on the Lewis acid sites, is more pronounced when the P content decreases, being in accordance with the previous results. At high CO dosages, a new band centred at 2132 cm^{-1}, associated with the physically adsorbed CO, is observed in all the samples.[38]

Another effect of the presence of extra-framework P species is the reduction of the N_2 adsorption capacity of the zeolite ITQ-52 (Figure S9), however, even at the highest P content, the zeolite ITQ-52 showed more than 70% of micropore volume (Table 2) of the essentially P-free ITQ-52 material, not observing a severe pore blocking.

3.4. Stability of Al in framework positions under steaming conditions

It is well known that the presence of extra-framework P-species improves the hydrothermal stability of the zeolite ZSM-5.[17][39] For exploring the effect of the P in the zeolite ITQ-52, the series of [Al_20]-ITQ-52 zeolites with different P content was studied before and after steaming treatment. The XRD diffraction patterns showed in Figure S10 confirm the stability of the zeolite framework after heating at 973 K in the presence of steam for 5 h.

The nature of the hydroxyl groups was studied by FT-IR spectroscopy. Figure 5 shows the FT-IR spectra of the ITQ-52 zeolites with different P content before and after steaming treatment. All the samples show a sharp band centred at 3735 cm^{-1}, attributed to the stretching vibration of the terminal silanols and a band centred at 3604 cm^{-1} that is generally assigned to the stretching vibration of the acid bridging hydroxyl groups Si-OH-Al.[37] The samples with a P/Al ratio lower than 1.0 show another band centred at 3575 cm^{-1} that was assigned to bridging hydroxyl groups Si-OH-Al located in a different environment,[40] in accordance with the results obtained in the ^{27}Al MAS NMR spectroscopy. The intensity of the band centred at 3655 cm^{-1} and the broad band at 3500 cm^{-1} increases with the P content. The first one was associated

with the stretching vibration of P-OH groups,[41] while the second one was assigned to disturbed Si-OH-Al groups that are interacting thought H-bonds with Si-OH or P-OH groups.[42] After steaming treatment, the intensity of the bands associated with the hydroxyl groups Si-OH-Al decreased, suggesting the loss of some acid sites during the steaming treatment. The intensity change is more pronounced in the sample with the lowest P content, while the presence of P seems to stabilize the acid sites under those harsh conditions.

The changes in the Al species after the steam treatment was followed by ^{27}Al MAS NMR spectroscopy (Figure 5). In the NMR spectra of the [Al_20]-ITQ-52 samples before steaming, resonances in the characteristic regions for the Al in tetrahedral and octahedral coordination are clearly visible for all the samples. The tetrahedral Al region of the zeolite with the lowest P content (P/Al = 0.08) is strongly modified after steaming. The intensity of the resonances at 54-56 ppm decreased notably, at the same time, a broad resonance centred at 50 ppm appeared. This region is characteristic of the Al in distorted tetrahedral coordination or pentacoordinated.[43] The sample with an intermediated P content (P/Al = 0.47) showed similar behaviour, but, the decrease in the intensity of the resonance corresponding to Al in framework positions is less pronounced. Besides, a resonance centred at 40 ppm which is generally associated to the presence of aluminophosphates,[44] can be observed suggesting the formation of local $AlPO_4$ species inside the cavities of the zeolite. The formation of $AlPO_4$ islands by the reaction of extra-framework P and Al leached from the framework has been previously reported for several zeolites.[45] On the opposite side, the sample with a P/Al ratio higher than 1 showed very close profiles before and after steaming treatment, confirming the Al stabilization by the presence of P.

3.5. Effect of the presence of extra-framework P in the MTO performance

The methanol to olefins (MTO) is one of the most important process to produce short-chain olefins.[46] The commercial catalyst SAPO-34 employed in this process shows a better performance in the reaction than the aluminosilicate analogue CHA, due to the medium acid strength and high thermal/hydrothermal stability. The presence of extra-framework P-species decreases the acid strength of the zeolites at the same time enhances the framework stability. The influence of the extra-framework P species in the MFI[47] and MCM-22[18] zeolites has been previously studied showing changes in the product selectivity and enhancement of the catalyst lifetime in the MTO reaction.

In order to examine the influence of the presence of P in the ITQ-52 zeolite in the MTO performance, Al- and Ga-containing samples with different P contents were employed as catalysts in the reaction. The methanol conversion and product selectivity in the MTO reaction at 673 K for the zeolites [B,Al_120]-ITQ-52 and [B,Ga_135]-ITQ-52 are shown in Figures 6 and 7, respectively. The presence of P has a significant influence on the catalyst lifetime and product selectivity. All the catalysts, except the zeolites with the highest P content, showed an initial total conversion of methanol. The low catalytic activity together the results obtained in the solid-state NMR and FT-IR study suggests that an excess of P species interacting with the Al or Ga atoms (P/Al=3.4 and P/Ga=3.6) could suppress most of the acid sites.

On the opposite side, the zeolites with a negligible P content showed faster catalyst deactivation and higher paraffin selectivity than the samples containing P-species. The alkanes are formed through the hydrogen transfer mechanism,[48] which is promoted by the Brönsted and Lewis acid sites following different mechanisms.[49][50] The zeolites without P-species, on one hand, show strong Brönsted acid sites and, on the other hand, during the heat treatments, small amount of extra-framework Al species that act as Lewis acid sites were formed. As a consequence, the formation of paraffins is enhanced, particularly, in the case of the [B,Al_120]-ITQ-52.

The presence of P has also an influence on the alkenes distribution. The propene/ethene ratio reached a maximum of 1.4 and 1.6 for [B,Al_120]-ITQ-52 and [B,Ga_135]-ITQ-52 with P/Al=0.17 and P/Ga=0.14, respectively. This enhancement in the propene selectivity over the ethene can be mainly explained by the low propane formation by the hydrogen transfer mechanism. These samples also showed the longest catalytic life, highlighting the importance of finding a P content value in which the acid strength is optimal for the MTO reaction. The higher selectivity to light olefins (ethane, propene and butenes) observed for the zeolite [B,Ga_135]-ITQ-52, could be related with the weaker acid strength of the catalyst compared with the Al-containing material. The NH_3-TPD profile shows a higher NH_3 desorption temperature for the [B,Al_120]-ITQ-52 (Figure S11), indicating the presence of stronger acid sites than Ga-containing ITQ-52. The FT-IR spectra upon CO adsorption showed the same results, where the ΔvOH (CO) for the [B,Al]-ITQ-52 (314 cm^{-1}) was larger than that obtained for the [B,Ga]-ITQ-52 (285 cm^{-1}). The relatively fast catalyst deactivation could be related to the presence of the large cavities and the big crystals of the ITQ-52 prepared in fluoride media (Figure S6).

Recently, the correlation between the cage-defining ring size of a series of small pore zeolites and the light olefin selectivity was reported.[51] The zeolites were sorted out in four categories regarding the cage-defining ring size showing similar MTO performance behaviour. Although the zeolite ITQ-52 is not a small pore zeolite, it is formed by cavities accessible by four 8R and two 10R windows, having a cage-defining ring size of 14 tetrahedra with a maximum diameter of a sphere that can be included of 7.7Å. The relation between the light olefins selectivities obtained in the MTO reaction and the size of the zeolite ITQ-52 cage is consistent with the reported results.

4. Conclusions

B-, Al- and Ga-containing IFW-type metallosilicate zeolites, ITQ-52 were prepared by direct synthesis using the P-OSDA, 1,4-butanediylbis[tris(dimethylamino)]phosphonium hydroxide. The pure borosilicate (Si/B = 17.2) and aluminosilicate (Si/Al = 17.8) materials were crystallized, as well as, a series of solids which combined elements. The Ga-containing ITQ-52 was only obtained when B was added to the synthesis gel too, with a maximum Si/Ga ratio of 71. The use of a P-containing OSDA allowed to introduce extra-framework P-species during the synthesis, which content can be controlled by post-synthesis treatments. The solid NMR results showed that the phosphorus species remain inside the cavities of the zeolites interacting with the Al or Ga located in framework positions, which can adopt a reversible octahedral coordination. The presence of P enhanced the stability of the Al in framework positions under steaming conditions (973 K for 5 h) at the same time that lowered the acid strength of the catalysts, however, an excess of phosphorus significantly decreased the acidity and catalytic activity. P content is a compromise between the stability of the Al in framework positions and the activity in the MTO reaction. The optimum P content for the samples with Si/Al = 120 and Si/Ga = 135 were P/Al = 0.17 and P/Ga = 0.14, respectively, showing longer catalyst lifetime, the highest propene selectivity (higher than 35%) and low paraffin formation. The combination of the direct incorporation of Al and Ga in the ITQ-52 and the extra-framework P-species by direct synthesis allowed to obtain a catalyst with improved properties. The optimization of this process by using an appropriate combination of P and N-containing OSDA could allow controlling the final P content in the absence of secondary post-treatments, making the ITQ-52 zeolite a potential catalyst for methanol to light olefins reaction. Thus, our findings will contribute to the diversification of the IFW-type zeolite with 8- and 10-ring channels.

Appendices

Appendix A. Supplementary data

Acknowledgements

This work was supported by Tokyo Tech World Research Hub Initiative (WRHI) Program of Institute of Innovative Research, Tokyo Institute of Technology; MINECO of Spain through the Severo Ochoa (SEV-2016-0683) and RTI2018-101784-B-I00 projects.

References

[1] A. Corma, Inorganic Solid Acids and Their Use in Acid-Catalyzed Hydrocarbon Reactions, Chem. Rev. 95 (1995) 559–614. https://doi.org/10.1021/cr00035a006.

[2] J. Cejka, A. Corma, S. Zones, Zeolites and catalysis: synthesis, reactions and applications, John Wiley & Sons, 2010.

[3] http://www.iza-structure.org/databases/ (accessed September 26, 2020), (2020).

[4] F. Rey, J. Simancas, Beyond Nitrogen OSDAs, in: L. Gómez-Hortigüela (Ed.), Insights into Chem. Org. Struct. Agents Synth. Zeolitic Mater., 2018: pp. 103–138. https://doi.org/10.1007/430_2017_13.

[5] S. Sáez-Ferre, C.W. Lopes, J. Simancas, A. Vidal-Moya, T. Blasco, G. Agostini, G. Mínguez Espallargas, J.L. Jordá, F. Rey, P. Oña-Burgos, Use of Alkylarsonium Directing Agents for the Synthesis and Study of Zeolites, Chem. – A Eur. J. 25 (2019) 16390–16396. https://doi.org/10.1002/chem.201904043.

[6] T.V. Whittam, Zeolites., DE2643929A1, 1977.

[7] G.T. Kokotailo, P. Chu, S.L. Lawton, W.M. Meier, Synthesis and structure of synthetic zeolite ZSM-11, Nature. 275 (1978) 119–120. https://doi.org/10.1038/275119a0.

[8] E. Mitani, Y. Yamasaki, N. Tsunoji, M. Sadakane, T. Sano, Synthesis of phosphorus-modified AFX zeolite using a dual-template method with tetraethylphosphonium hydroxide as phosphorus modification agent, Microporous Mesoporous Mater. 267 (2018) 192–197. https://doi.org/https://doi.org/10.1016/j.micromeso.2018.03.033.

[9] Y. Kakiuchi, T. Tanigawa, N. Tsunoji, Y. Takamitsu, M. Sadakane, T. Sano, Phosphorus modified small-pore zeolites and their catalytic performances in ethanol conversion and NH3-SCR reactions, Appl. Catal. A Gen. 575 (2019) 204–213. https://doi.org/https://doi.org/10.1016/j.apcata.2019.02.026.

[10] E. Mitani, N. Tsunoji, M. Sadakane, T. Sano, Synthesis of GME zeolite with high porosity by hydrothermal conversion of FAU zeolite using a dual-template method with tetraethylphosphonium and N,N-dimethyl-3,5-dimethylpiepridinium hydroxides, J. Porous Mater. 26 (2019) 1345–1352. https://doi.org/10.1007/s10934-019-00725-x.

[11] D.L. Dorset, G.J. Kennedy, K.G. Strohmaier, M.J. Diaz-Cabañas, F. Rey, A. Corma, P-Derived Organic Cations as Structure-Directing Agents: Synthesis of a High-Silica Zeolite (ITQ-27) with a Two-Dimensional 12-Ring Channel System, J. Am. Chem. Soc. 128 (2006) 8862–8867. https://doi.org/10.1021/ja061206o.

[12] A. Corma, M.J. Diaz-Cabañas, J.L. Jorda, F. Rey, G. Sastre, K.G. Strohmaier, A Zeolitic Structure (ITQ-34) with Connected 9- and 10-Ring Channels Obtained with Phosphonium Cations as Structure Directing Agents, J. Am. Chem. Soc. 130 (2008) 16482–16483. https://doi.org/10.1021/ja806903c.

[13] A. Corma, M.J. Diaz-Cabañas, J. Jiang, M. Afeworki, D.L. Dorset, S.L. Soled, K.G. Strohmaier, Extra-large pore zeolite (ITQ-40) with the lowest framework density containing double four- and double three-rings., Proc. Natl. Acad. Sci. U. S. A. 107 (2010) 13997–14002. https://doi.org/10.1073/pnas.1003009107.

[14] M. Hernández-Rodríguez, J.L. Jordá, F. Rey, A. Corma, Synthesis and Structure

Determination of a New Microporous Zeolite with Large Cavities Connected by Small Pores, J. Am. Chem. Soc. 134 (2012) 13232–13235. https://doi.org/10.1021/ja306013k.

[15] Y. Yun, M. Hernández, W. Wan, X. Zou, J.L. Jordá, A. Cantín, F. Rey, A. Corma, The first zeolite with a tri-directional extra-large 14-ring pore system derived using a phosphonium-based organic molecule, Chem. Commun. 51 (2015) 7602–7605. https://doi.org/10.1039/C4CC10317C.

[16] R. Simancas, D. Dari, N. Velamazán, M.T.M.T. Navarro, A. Cantín, J.L. Jordá, G. Sastre, A. Corma, F. Rey, Modular organic structure-directing agents for the synthesis of zeolites., Science. 330 (2010) 1219–1222. https://doi.org/10.1126/science.1196240.

[17] T. Blasco, A. Corma, J. Martínez-Triguero, Hydrothermal stabilization of ZSM-5 catalytic-cracking additives by phosphorus addition, J. Catal. 237 (2006) 267–277. https://doi.org/10.1016/j.jcat.2005.11.011.

[18] X. Wang, W. Dai, G. Wu, L. Li, N. Guan, M. Hunger, Phosphorus modified HMCM-22: Characterization and catalytic application in methanol-to-hydrocarbons conversion, Microporous Mesoporous Mater. 151 (2012) 99–106. https://doi.org/10.1016/j.micromeso.2011.11.008.

[19] H.E. van der Bij, B.M. Weckhuysen, Phosphorus promotion and poisoning in zeolite-based materials: synthesis, characterisation and catalysis, Chem. Soc. Rev. 44 (2015) 7406–7428. https://doi.org/10.1039/C5CS00109A.

[20] R. Simancas, J.L. Jordá, F. Rey, A. Corma, A. Cantín, I. Peral, C. Popescu, A New Microporous Zeolitic Silicoborate (ITQ-52) with Interconnected Small and Medium Pores, J. Am. Chem. Soc. 136 (2014) 3342–3345. https://doi.org/10.1021/ja411915c.

[21] S. Smeets, L.B. McCusker, C. Baerlocher, D. Xie, C.-Y. Chen, S.I. Zones, SSZ-87: A Borosilicate Zeolite with Unusually Flexible 10-Ring Pore Openings, J. Am. Chem. Soc. 137 (2015) 2015–2020. https://doi.org/10.1021/ja512411b.

[22] J. Simancas, R. Simancas, P.J. Bereciartua, J.L. Jorda, F. Rey, A. Corma, S. Nicolopoulos, P. Pratim Das, M. Gemmi, E. Mugnaioli, Ultrafast Electron Diffraction Tomography for Structure Determination of the New Zeolite ITQ-58, J. Am. Chem. Soc. 138 (2016) 10116–10119. https://doi.org/10.1021/jacs.6b06394.

[23] P. Wagner, S.I. Zones, M.E. Davis, R.C. Medrud, SSZ-35 and SSZ-44: two related zeolites containing pores circumscribed by ten- and eighteen-membered rings, Angew. Chem., Int. Ed. 38 (1999) 1269–1272. https://doi.org/10.1002/(sici)1521-3773(19990503)38:9<1269::aid-anie1269>3.0.co;2-3.

[24] M. Yoshioka, T. Yokoi, T. Tatsumi, Development of the CON-type Aluminosilicate Zeolite and Its Catalytic Application for the MTO Reaction, ACS Catal. 5 (2015) 4268–4275. https://doi.org/10.1021/acscatal.5b00692.

[25] T. Yokoi, M. Yoshioka, H. Imai, T. Tatsumi, Diversification of RTH-type zeolite and its catalytic application., Angew. Chemie Int. Ed. 48 (2009) 9884–7. https://doi.org/10.1002/anie.200905214.

[26] R.W. Broach, E.P. Boldingh, D.-Y. Jan, G.J. Lewis, J.G. Moscoso, J.C. Bricker, Tailoring zeolite morphology by Charge Density Mismatch for aromatics processing, J. Catal. 308 (2013) 142–153. https://doi.org/https://doi.org/10.1016/j.jcat.2013.05.034.

[27] A. Boultif, D. Louër, Powder pattern indexing with the dichotomy method, J. Appl. Crystallogr. 37 (2004) 724–731. https://doi.org/10.1107/S0021889804014876.

[28] J. Rodriguez-Carvajal, FULLPROF: a program for Rietveld refinement and pattern matching analysis, in: Satell. Meet. Powder Diffr. XV Congr. IUCr, 1990: p. 127.

[29] S.-J. Hwang, C.-Y. Chen, S.I. Zones, Boron sites in borosilicate zeolites at various stages of hydration studied by solid state NMR spectroscopy, J. Phys. Chem. B. 108 (2004) 18535–18546.

[30] S. Sklenak, J. Dědeček, C. Li, B. Wichterlová, V. Gábová, M. Sierka, J. Sauer, Aluminum

Siting in Silicon-Rich Zeolite Frameworks: A Combined High-Resolution 27Al NMR Spectroscopy and Quantum Mechanics / Molecular Mechanics Study of ZSM-5, Angew. Chemie Int. Ed. 46 (2007) 7286–7289. https://doi.org/10.1002/anie.200702628.

[31] J. Dědeček, Z. Sobalík, B. Wichterlová, Siting and Distribution of Framework Aluminium Atoms in Silicon-Rich Zeolites and Impact on Catalysis, Catal. Rev. 54 (2012) 135–223. https://doi.org/10.1080/01614940.2012.632662.

[32] R.D. Shannon, Revised effective ionic radii and systematic studies of interatomic distances in halides and chalcogenides, Acta Crystallogr. Sect. A. 32 (1976) 751–767. https://doi.org/10.1107/S0567739476001551.

[33] A. Arnold, S. Steuernagel, M. Hunger, J. Weitkamp, Insight into the dry-gel synthesis of gallium-rich zeolite [Ga]Beta, Microporous Mesoporous Mater. 62 (2003) 97–106. https://doi.org/https://doi.org/10.1016/S1387-1811(03)00397-4.

[34] A. Kuperman, S. Nadimi, S. Oliver, G.A. Ozin, J.M. Garcés, M.M. Olken, Non-aqueous synthesis of giant crystals of zeolites and molecular sieves, Nature. 365 (1993) 239–242. https://doi.org/10.1038/365239a0.

[35] H.E. van der Bij, B.M. Weckhuysen, Local silico-aluminophosphate interfaces within phosphated H-ZSM-5 zeolites, Phys. Chem. Chem. Phys. 16 (2014) 9892–9903. https://doi.org/10.1039/C3CP54791D.

[36] C.A. Emeis, Determination of integrated molar extinction coefficients for infrared absorption bands of pyridine adsorbed on solid acid catalysts, J. Catal. 141 (1993) 347–354.

[37] J.A. Lercher, C. Gründling, G. Eder-Mirth, Infrared studies of the surface acidity of oxides and zeolites using adsorbed probe molecules, Catal. Today. 27 (1996) 353–376. https://doi.org/https://doi.org/10.1016/0920-5861(95)00248-0.

[38] A. Zecchina, G. Spoto, S. Bordiga, Probing the acid sites in confined spaces of

microporous materials by vibrational spectroscopy, Phys. Chem. Chem. Phys. 7 (2005) 1627–1642. https://doi.org/10.1039/B418763F.

[39] Y.-J. Lee, J.M. Kim, J.W. Bae, C.-H. Shin, K.-W. Jun, Phosphorus induced hydrothermal stability and enhanced catalytic activity of ZSM-5 in methanol to DME conversion, Fuel. 88 (2009) 1915–1921. https://doi.org/https://doi.org/10.1016/j.fuel.2009.04.007.

[40] F. Wakabayashi, J. Kondo, A. Wada, K. Domen, C. Hirose, FT-IR studies of the interaction between zeolitic hydroxyl groups and small molecules. 1. Adsorption of nitrogen on H-mordenite at low temperature, J. Phys. Chem. 97 (1993) 10761–10768. https://doi.org/10.1021/j100143a040.

[41] A. Janin, J.C. Lavalley, E. Benazzi, C. Schott-Darie, H. Kessler, Acidity of cloverite, Stud. Surf. Sci. Catal. 94 (1995) 124–130. https://doi.org/https://doi.org/10.1016/S0167-2991(06)81213-9.

[42] B. Gil, S.I. Zones, S.-J. Hwang, M. Bejblova, J. Cejka, M. Bejblová, J. Čejka, Acidic Properties of SSZ-33 and SSZ-35 Novel Zeolites: a Complex Infrared and MAS NMR Study, J. Phys. Chem. C. 112 (2008) 2997–3007. https://doi.org/10.1021/jp077687v.

[43] J. Huang, Y. Jiang, V.R. Marthala, B. Thomas, E. Romanova, M. Hunger, Characterization and Acidic Properties of Aluminum-Exchanged Zeolites X and Y, J. Phys. Chem. C. 112 (2008) 3811–3818. https://doi.org/10.1021/jp7103616.

[44] B. Zibrowius, E. Löffler, M. Hunger, Multinuclear MAS n.m.r. and i.r. spectroscopic study of silicon incorporation into SAPO-5, SAPO-31, and SAPO-34 molecular sieves, Zeolites. 12 (1992) 167–174. https://doi.org/https://doi.org/10.1016/0144-2449(92)90079-5.

[45] A.F. Costa, H.S. Cerqueira, J.M. Ferreira, N.M. Ruiz, S.M. Menezes, BEA and MOR as additives for light olefins production, Appl. Catal. A Gen. 319 (2007) 137–143. https://doi.org/https://doi.org/10.1016/j.apcata.2006.11.027.

[46] P. Tian, Y. Wei, M. Ye, Z. Liu, Methanol to Olefins (MTO): From Fundamentals to

Commercialization, ACS Catal. 5 (2015) 1922–1938. https://doi.org/10.1021/acscatal.5b00007.

[47] M. Dyballa, E. Klemm, J. Weitkamp, M. Hunger, Effect of Phosphate Modification on the Brønsted Acidity and Methanol-to-Olefin Conversion Activity of Zeolite ZSM-5, Chem. Ing. Tech. 85 (2013) 1719–1725. https://doi.org/10.1002/cite.201300066.

[48] S. Ilias, A. Bhan, Mechanism of the Catalytic Conversion of Methanol to Hydrocarbons, ACS Catal. 3 (2013) 18–31. https://doi.org/10.1021/cs3006583.

[49] M. Boronat, P. Viruela, A. Corma, Ab initio and density-functional theory study of zeolite-catalyzed hydrocarbon reactions: hydride transfer, alkylation and disproportionation, Phys. Chem. Chem. Phys. 2 (2000) 3327–3333. https://doi.org/10.1039/B002013N.

[50] S. Müller, Y. Liu, F.M. Kirchberger, M. Tonigold, M. Sanchez-Sanchez, J.A. Lercher, Hydrogen Transfer Pathways during Zeolite Catalyzed Methanol Conversion to Hydrocarbons, J. Am. Chem. Soc. 138 (2016) 15994–16003. https://doi.org/10.1021/jacs.6b09605.

[51] J.H. Kang, F.H. Alshafei, S.I. Zones, M.E. Davis, Cage-Defining Ring: A Molecular Sieve Structural Indicator for Light Olefin Product Distribution from the Methanol-to-Olefins Reaction, ACS Catal. 9 (2019) 6012–6019. https://doi.org/10.1021/acscatal.9b00746.

Footnotes

[1] Present address: Chemical System Engineering, School of Engineering, The University of Tokyo, Tokyo, 1138656, Japan.

Tables

Table 1. Chemical composition and unit cell volume of the as-made ITQ-52 zeolites.

Sample	Si/B	Si/Al(Ga)	Si/(B+Al(Ga))	P/(B+Al(Ga))	Si/u.c.	B/u.c.	Al(Ga)/u.c.	P/u.c.	Unit cell volume (Å^3)
[B]-ITQ-52	17.2	-	17.2	1.1	60.5	3.5	-	3.8	3838
[B,Al_206]-ITQ-52	19.0	205.9	17.4	1.1	60.5	3.2	0.3	3.9	3849
[B,Al_91]-ITQ-52	23.2	90.9	18.5	1.2	60.7	2.6	0.7	3.9	3862
[B,Al_58]-ITQ-52	31.5	58.5	20.5	1.3	61.0	1.9	1.1	3.8	3879
[B,Al_21]-ITQ-52	113.1	20.8	17.6	1.2	60.6	0.5	2.9	3.9	3935
[Al_19]-ITQ-52	-	17.8	17.8	1.2	60.6	-	3.4	4.2	3950
[B,Ga_291]-ITQ-52	25.7	290.5	21.8	1.4	61.4	2.4	0.2	3.6	3857
[B,Ga_137]-ITQ-52	26.1	137.2	21.9	1.4	61.2	2.3	0.5	3.9	3866
[B,Ga_82]-ITQ-52	33.8	81.8	18.5	1.4	61.4	1.8	0.8	3.6	3875
[B,Ga_71]-ITQ-52	36.6	70.5	18.0	1.4	61.4	1.7	0.9	3.6	3882

Table 2. Chemical analyses and acid and textural properties of the zeolite [Al_20]-ITQ-52 having different P content before and after steaming treatments at 973 K.

Sample	Treatment	Si/Al	P/Al	A_{BET} (m^2/g)[a]	V_{mic} (cm^3/g)[b]	L_{423} (mmol py/g)[c]	B_{423} (mmol py/g)[c]
[Al_20]-ITQ-52	-	21.64	1.33	-	-		-
[Al_20]-ITQ-52_AT	923 K, air	21.96	1.35	385	0.153	0.007	0.043
[Al_20]-ITQ-52_AT_ST	Steamed 973 K, 5 h	21.51	1.3	376	0.161	0.007	0.037
[Al_20]-ITQ-52_ATw303	923 K, air + NH_4Ac 303 K	21.49	1.06	420	0.165	0.040	0.203
[Al_20]-ITQ-52_ATw303_ST	Steamed 973 K, 5 h	21.23	1.03	397	0.168	0.033	0.157
[Al_20]-ITQ-52_HT	873 K, H_2/N_2	21.68	0.47	515	0.238	0.098	0.607
[Al_20]-ITQ-52_HT_ST	Steamed 973 K, 5 h	21.37	0.46	499	0.229	0.177	0.408
[Al_20]-ITQ-52_HTw363	873 K, H_2/N_2 + NH_4Ac 363 K	21.25	0.08	511	0.221	0.402	0.604
[Al_20]-ITQ-52_HTw363_ST	Steamed 973 K, 5 h	21.06	0.05	487	0.202	0.252	0.335

[a] calculated using the Brunauer, Emmett and Teller (BET) method. [b] determined from the N_2 adsorption isotherm by applying the *t*-plot method. [c] L_{423} and B_{423} were calculated from the integrated absorbance of the band centred at 1450 cm^{-1} (Lewis) and 1550 cm^{-1} (Brönsted), respectively, in the FT-IR spectra.

Figure captions

Figure 1. Unit cell volume (left) and relative variation of the *a* (■), *b* (○) and *c* (●) axes with respect to those of the [B]-ITQ-52 (right) with the Al content per unit cell.

Figure 2. ^{11}B, ^{27}Al and ^{31}P MAS NMR spectra of the zeolite [B,Al_91]-ITQ-52 as-made (a), after heating at 923 K under air, [B,Al_91]-ITQ-52_AT (b), after heating at 873 K under a stream of H_2/N_2, [B,Al_91]-ITQ-52_HT (c), and after heating at 873 K under a stream of H_2/N_2, washing at 363 K with an aqueous solution of ammonium acetate and calcined at 823 K in air, [B,Al_91]-ITQ-52_HT_w363 (d).

Figure 3. ^{11}B, ^{71}Ga and ^{31}P MAS NMR spectra of the zeolite [B,Ga_82]-ITQ-52 as-made (a), after heating at 923 K under air, [B,Ga_82]-ITQ-52_AT (b), after heating at 873 K under a stream of H_2/N_2, [B,Ga_82]-ITQ-52_HT (c), after heating at 873 K under a stream of H_2/N_2, washing at 363 K with an aqueous solution of ammonium acetate and calcined at 823 K in air, [B,Ga_82]-ITQ-52_HT_w363 (d).

Figure 4. Differential FT-IR spectra for ν(OH) (A) and ν(CO) (B) regions of the CO-adsorbed zeolite [Al_20]-ITQ-52 heated at 923 K in air, [Al_20]-ITQ-52_AT (a), heated at 923 K in air and washed with ammonium acetate at 303 K, [Al_20]-ITQ-52_ATw303 (b), heated at 873 K in H_2/N_2, [Al_20]-ITQ-52_HT (c) and heated at 873 K in H_2/N_2 and washed at 363 K with ammonium acetate, [Al_20]-ITQ-52_HTw363 (d).

Figure 5. FT-IR spectra (left) and ^{27}Al MAS NMR spectra (right) of the zeolite [Al_20]-ITQ-52 heated at 923 K under air (a) and subsequently washed with ammonium acetate at 303 K (b),

heated at 873 K under H_2/N_2 (c) and subsequently washed with ammonium acetate at 363 K (d) before (line) and after (dots) steaming treatment at 973 K for 5 h.

Figure 6. Methanol conversion and product selectivity in the MTO reaction at 673 K for the [B,Al_120]-ITQ-52 with different P content.

Figure 7. Methanol conversion and product selectivity in the MTO reaction at 673 K for the [B,Ga_135]-ITQ-52 with different P content.

Figures

Figure 1.

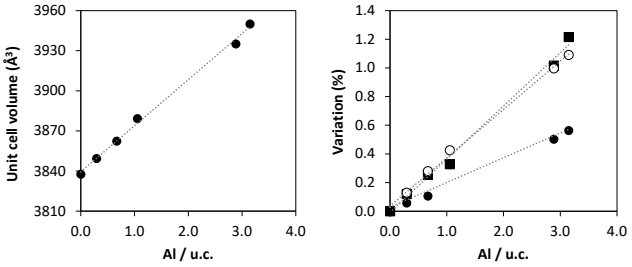

Figure 2.

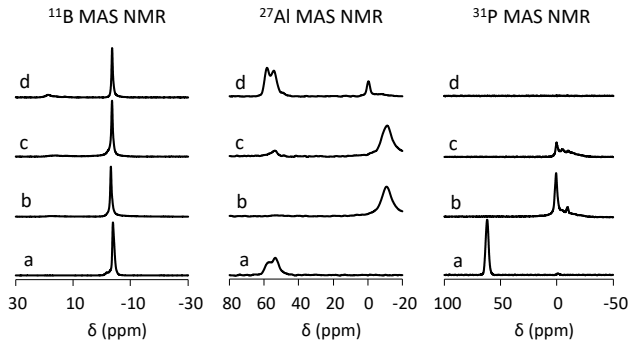

Figure 3.

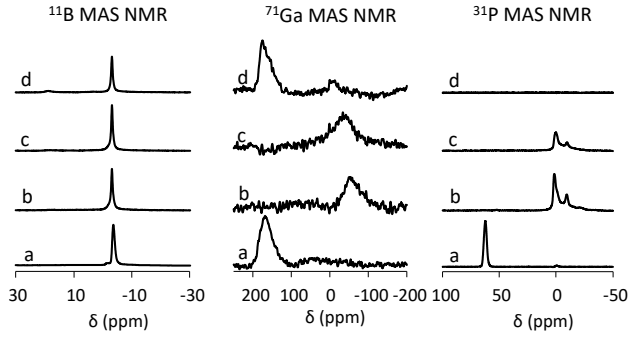

Figure 4.

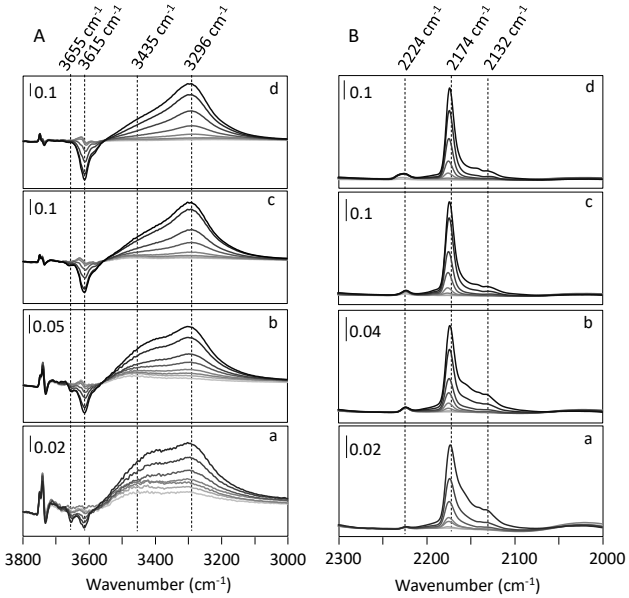

Figure 5.

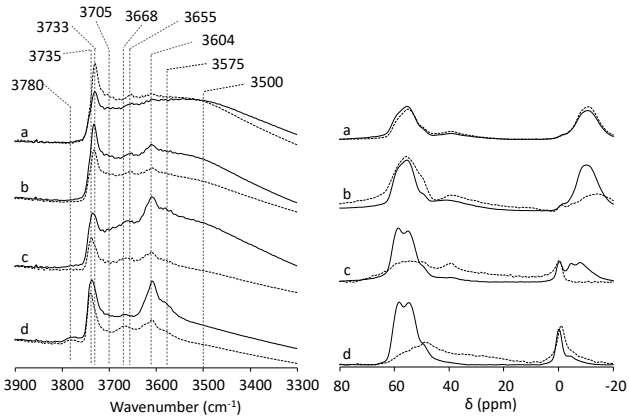

Figure 6.

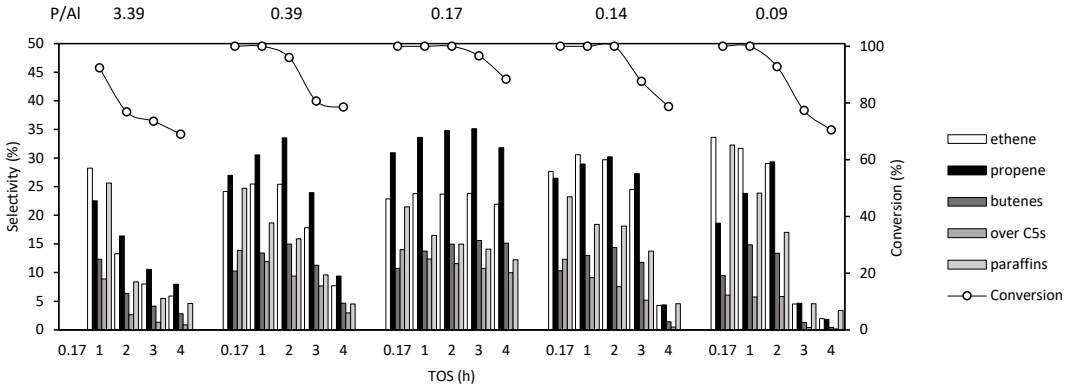

Figure 7.